



Delft University of Technology

## The challenge of catalyst prediction

Van Santen, Rutger A.; Sengar, A.; Steur, Erik

**DOI**

[10.1039/C7FD00208D](https://doi.org/10.1039/C7FD00208D)

**Publication date**

2018

**Document Version**

Final published version

**Published in**

Faraday Discussions

**Citation (APA)**

Van Santen, R. A., Sengar, A., & Steur, E. (2018). The challenge of catalyst prediction. *Faraday Discussions*, 208, 35-52. <https://doi.org/10.1039/C7FD00208D>

**Important note**

To cite this publication, please use the final published version (if applicable). Please check the document version above.

**Copyright**

Other than for strictly personal use, it is not permitted to download, forward or distribute the text or part of it, without the consent of the author(s) and/or copyright holder(s), unless the work is under an open content license such as Creative Commons.

**Takedown policy**

Please contact us and provide details if you believe this document breaches copyrights. We will remove access to the work immediately and investigate your claim.

# The challenge of catalyst prediction

Rutger A. van Santen, \*<sup>ab</sup> Aditya Sengar<sup>c</sup> and Erik Steur<sup>d</sup>

Received 17th November 2017, Accepted 15th January 2018

DOI: 10.1039/c7fd00208d

New insights and successful use of computational catalysis are highlighted. This is within the context of remaining issues that prevent theoretical catalysis to be fully predictive of catalyst performance. A major challenge is to include in modelling studies the transient initiation as well as deactivation processes of the catalyst. We will illustrate this using as an example for solid acid catalysis, the alkylation process, and for transition metal catalysis, the Fischer–Tropsch reaction. For the alkylation reaction of isobutane and alkene, an important reaction for high octane gasoline, we will present a deactivation model. For the Fischer–Tropsch reaction, which converts synthesis gas into gasoline grade molecules, we discuss structural reorganization of the catalyst induced by reaction.

## 1 Introduction

One of the holy grails of computational catalysis is to change catalysis from a science dominated by empirical correlation into a science based on predictive mechanistic modelling.

Here we will investigate what is the current state of affairs of the computational catalysis project. We will argue that, notwithstanding major advances in understanding the kinetics of many systems, great challenges remain. This is due to complex feedback loops not only between the elementary reactions that take place, but also because of their strong coupling with the inorganic chemistry of the catalytic system. For practical invention the empirical approach remains indispensable and highly useful. Computational catalysis science plays an increasing role to refine and optimize such experimental catalysis programs.

A major reason for this state of affairs is that for many systems state of the catalyst surface may change during reaction. The structural changes of the Fischer–Tropsch catalyst that we will discuss illustrate this.

<sup>a</sup>Institute for Complex Molecular Systems, Eindhoven University of Technology, 5612AZ Eindhoven, The Netherlands. E-mail: r.a.v.santen@tue.nl

<sup>b</sup>Laboratory of Inorganic Materials Chemistry, Department of Chemistry and Chemical Engineering, Eindhoven University of Technology, 5612AZ Eindhoven, The Netherlands

<sup>c</sup>Multi-Phase Flows Group, Department of Chemistry and Chemical Engineering, Eindhoven University of Technology, 5612AZ Eindhoven, The Netherlands

<sup>d</sup>Delft Center for Systems and Control, Delft Technical University, The Netherlands

The catalyst reactive life can be distinguished in several often closely inter-linked stages: reaction initiation, stable operation and catalyst deactivation. Not only the inorganic chemistry of the catalyst surface may change through the three stages, but also the mechanism of the reaction. The latter we will illustrate for the alkylation reaction of isobutane and propylene catalyzed by solid acids. We will present kinetics modelling results of this reaction that includes the three reactivity changes of initiation, propagation and deactivation in an integrated way.

Advances in computational modelling have been impressive, beginning with the first principle quantum-chemical calculation of the propylene insertions step in the Ziegler–Natta polymerization reaction catalyzed by  $\text{TiCl}_3$  of Clementi *et al.*<sup>1</sup> up to the Sabatier volcano type first principle microkinetics prediction of composition dependence of the ammonia synthesis reaction by Dahl *et al.*<sup>2</sup>

Force field based molecular mechanics and dynamics approaches are useful to study structural changes of the catalytic systems. Force field based methods originate from solid state chemistry and have been explored in early simulations by Thomas and Catlow<sup>3</sup> to predict the optimum nanopore structure and dimensions of microporous zeolites for a particular reaction. Force fields derived from quantum-chemical calculations can be applied also to study complex catalytic reactions and reorganization of catalyst structure.<sup>4,5</sup>

Whereas microkinetics simulations are usually done assuming one or two reaction rates to be rate controlling,<sup>6</sup> current state of the art computational catalysis investigating catalytic reactivity–structure/composition relations can also be done with microkinetics simulations, that include all of the elementary reaction steps.<sup>7,8</sup>

The elementary reaction constants can be deduced from first principles methods, mainly DFT-based quantum-chemical calculations. Development of improved methods with increasingly better accuracy is rapid.<sup>9–12</sup> Computational studies have become available that do not limit themselves to only a few reaction steps, but rather elementary reaction steps of the full catalytic cycle are considered.<sup>7,8,13</sup>

Microkinetics simulations do not only deliver overall reaction rates, but also predict the composition of the surface overlayer that develops during reactions. Surface thermodynamic techniques<sup>14</sup> are available to calculate the equilibrium composition of a surface overlayer as a function of reaction environment. Molecular dynamics approaches are useful to study the surface reconstruction of transition metals or oxides, but have to be done separately from kinetics simulations because of the different timescales that are involved.

An important simulation method for the calculation of adsorption isotherms of complex mixtures of organic molecules or reaction intermediates in zeolite micropores based on fitted force fields is the configurational-bias Monte Carlo approach. It has been used to successfully predict the selectivity of the hydro-cracking reaction.<sup>15</sup>

The reaction mechanism and state of the catalyst surface for a reaction are interdependent. The mechanism of a reaction defines the network of elementary reactions that connect reactants with products. The interdependence of reaction mechanism and surface state makes catalyst performance prediction an iterative problem. As we will see it is the main reason why for many reactions there is still no consensus on its reaction mechanism. This constrains prediction of catalyst reaction–catalyst structure/composition relations.

In the next section we will discuss the interdependence of the different stages of catalyst reactivity. We will illustrate this with an analysis of the change in reaction mechanism in the initiation *versus* stationary propagation phase of the alkylation reaction of propylene and isobutane catalyzed by zeolitic solid acids. In particular, we will discuss a nonlinear catalyst deactivation model due to the changing reactivity of catalyst protons when partially deactivated.

In a following section we will highlight structural changes of transition metal catalysts for the Fischer–Tropsch reaction catalyzed by Co or Ru and their relation to the mechanism of the reaction.

We will conclude the paper with a Discussion and Conclusion section where we will summarize current controversies on the reaction mechanisms of a few additional selected reactions. We will emphasize the consequences for catalyst performance–structure/composition relations.

## 2 Solid acid catalysis, the alkylation reaction

An essential elementary reaction step in many solid acid catalyzed reactions is protonation of an unsaturated molecule, such as an alkene, that produces a carbenium ion. Some of these carbenium ions act as organo-catalytic intermediates in solid acid catalyzed reactions without direct involvement of the protons. Formation of these intermediate organo-catalytic molecules usually occurs in the initiation phase of the reaction. Examples of such reactions are the catalytic cracking reaction or the methanol to olefin reaction.<sup>16,17</sup>

In this section we will provide a kinetic analysis of a reaction cycle that includes initiation, propagation and deactivation for the alkylation reaction of isobutane and propylene catalyzed by a solid acid material.

The product of this reaction is a branched C<sub>7</sub> or C<sub>8</sub> alkane. The reaction is of interest as the alkylation reaction catalyzed by liquid sulfuric acid or hydrogen fluoride is widely applied to produce high octane gasoline and there is a need to replace the fluid acid by a solid acid.<sup>18</sup>

To reduce the complexity of the kinetics analysis we will use a reduced, simplified model of the kinetics of the reaction, that is schematically shown in Fig. 1. We only consider production of one of the C<sub>7</sub> isomers and ignore the auto alkylation reaction that produces the C<sub>8</sub> molecules.<sup>19</sup> For a detailed discussion and complete first principles modelling of the reaction see ref. 20 and 21 that contain a compilation of quantum-chemically calculated reaction intermediate energies as well as corresponding elementary reaction steps.

We present here the transient solutions of the kinetics of the reaction cycle presented in Fig. 1. In this minimalistic reaction scheme, several elementary reaction steps are combined into one “elementary” reaction step.

The initiation reaction, with combined reaction rate  $k_1$  in Fig. 1, generates the isobutyl cation  $iC_4^+$  that can be considered an organo-catalytic intermediate molecule of the reaction. It is formed after protonation of ethylene and subsequent reaction with isobutane. Propane is a coproduct of the initiation reaction. Direct competition with propylene oligomerisation is not considered here, but is discussed in an extended model of the alkylation reaction to be published elsewhere.<sup>27</sup>

In the propagation reaction cycle, the C<sub>7</sub><sup>+</sup> carbenium ion is formed by reaction of the isobutyl cation with propylene (with rate constant  $k_2$ ). The desired product

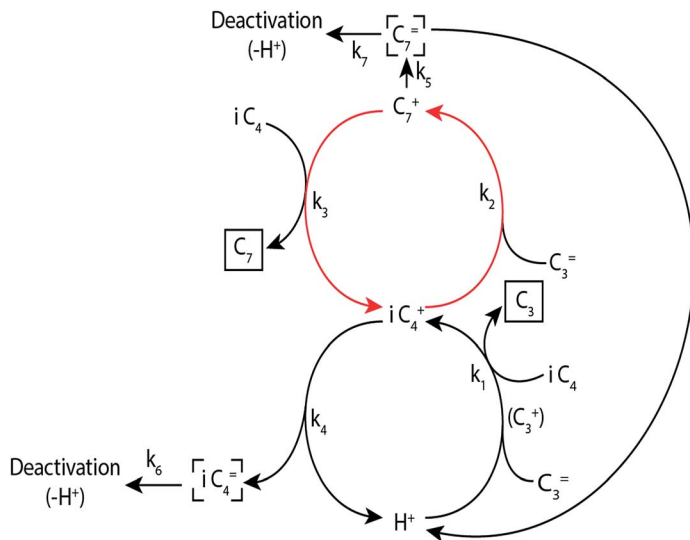


Fig. 1 Minimalistic schematic model of the initiation, propagation and deactivation reaction cycles of the alkylation process. Initiation, propagation and deactivation are closely entangled.  $[C_3]$ ,  $[C_7]$  are products;  $[iC_4^-]$ ,  $[C_7^-]$  are undesirable intermediates. Protons are consumed in the deactivation reactions.<sup>22,23</sup>

$C_7$ , the alkylate, is formed by a subsequent hydride transfer reaction with another isobutane molecule (with rate constant  $k_3$ ). This regenerates the isobutyl cation. In this propagation cycle the proton is not back donated to the solid.

Non selective catalysis occurs when  $C_7^-$  or  $iC_4^-$  alkenes are formed and a proton is back donated to the solid. This not only fuels the initiation reaction and non-selective propane formation, but it also initiates deactivation reactions. We describe that by the single lumped kinetics rate parameters  $k_6$  and  $k_7$ .

Catalyst deactivation can occur by the paring reaction,<sup>24</sup> by which a complex series of hydride transfer reactions and additional alkylation reactions of the  $C_7^+$  cation lead to stable cyclopentanyl cations, and which deactivates the catalyst because they consume a highly reactive proton. Alternatively the alkenes can oligomerize to give aromatic hydrocarbons. This reaction is less proton reactivity demanding.

The reaction only becomes stationary when deactivation is ignored. Then the steady state solutions to the reaction are readily found. The selectivity of the reaction, defined as the percentage of isobutane converted *versus*  $C_7$  production is given by eqn (1a):

$$S_D = \frac{\frac{d}{dt}[C_7]}{\frac{d}{dt}[C_3] + \frac{d}{dt}[C_7]} \quad (1a)$$

$$S_D = \frac{k_2 k_3 [iC_4] [C_3^-]}{k_2 k_5 [C_3^-] + k_3 k_4 [iC_4] + k_4 k_5 + k_2 k_3 [iC_4] [C_3^-]}$$

The steady state production rate of  $C_7$  production is given by eqn (1b):

$$\frac{d}{dt}[C_7] = \frac{k_1 k_2 k_3 [iC_4]^2 [C_3^-]^2}{k_2 k_5 [C_3^-] + k_3 k_4 [iC_4] + k_4 k_5 + k_1 [iC_4] [C_3^-] (k_3 [iC_4] + k_5 + k_2 [C_3^-])}$$

$$\frac{d}{dt}[C_7] \approx \frac{k_2 k_3 [iC_4] [C_3^-]}{k_2 [C_3^-] + k_3 [iC_4]} (k_1 \ll k_4 k_5) \quad (1b)$$

The rate constants used in eqn (1) are as indicated in Fig. 1. The selectivity of the reaction (eqn (1a)), is independent of initiation kinetics. In order to have high selectivity of reaction, rates of alkene production have to be slow compared with the rates of reactions that participate in the propagation cycle.

The rate of  $C_7$  production is only independent of the initiation reaction rate when the rate of initiation reaction is fast compared to the rates of carbenium ion deprotonation. The rate controlling step of the initiation reaction is the hydride transfer reaction of isobutane and propyl cation. The rate of the hydride transfer reaction as well as C–C bond formation between isobutyl cation and propylene has to be fast compared with the rate of olefin deprotonation for stable catalysis. This condition is only for solid acids with high proton reactivity and strong competitive adsorption of reactants.<sup>21</sup>

In Fig. 2 and 3, we compare the product distributions of the reaction cycle in Fig. 1 as deduced from the solutions of the corresponding kinetics equations. Since catalyst deactivating reactions are included, the reaction now is transient. The results presented in Fig. 2 are for a solid acid that contains only one type of proton and its reactivity is independent of the degree of deactivation *versus* the case presented in Fig. 3, when proton reactivity becomes non-uniform by deactivation and two protons of different reactivity are considered.

Fig. 2 shows that the relative site concentrations of  $iC_4^+$  and  $C_7^+$  are proportional to the rate of  $C_7$  and  $iC_4^-$  production. Also the changes in proton concentration  $H_1^+$  and deactivated sites  $H_0^+$  are shown. Different time regimes have been chosen to discriminate between initiation, quasi-stable and deactivation regimes.

The choice of default parameters is consistent with the activity of the La–Y zeolite system studied in ref. 21, where it was found that the reaction rate constants  $k_1$ , and  $k_3$  are comparable.

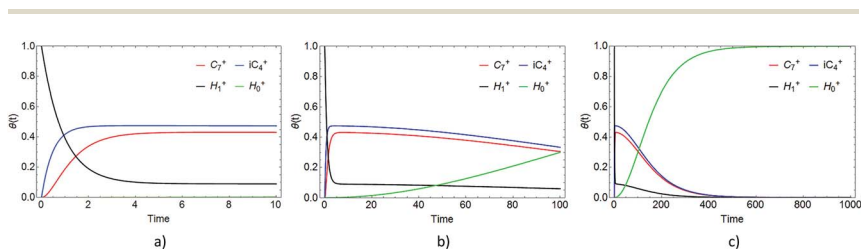
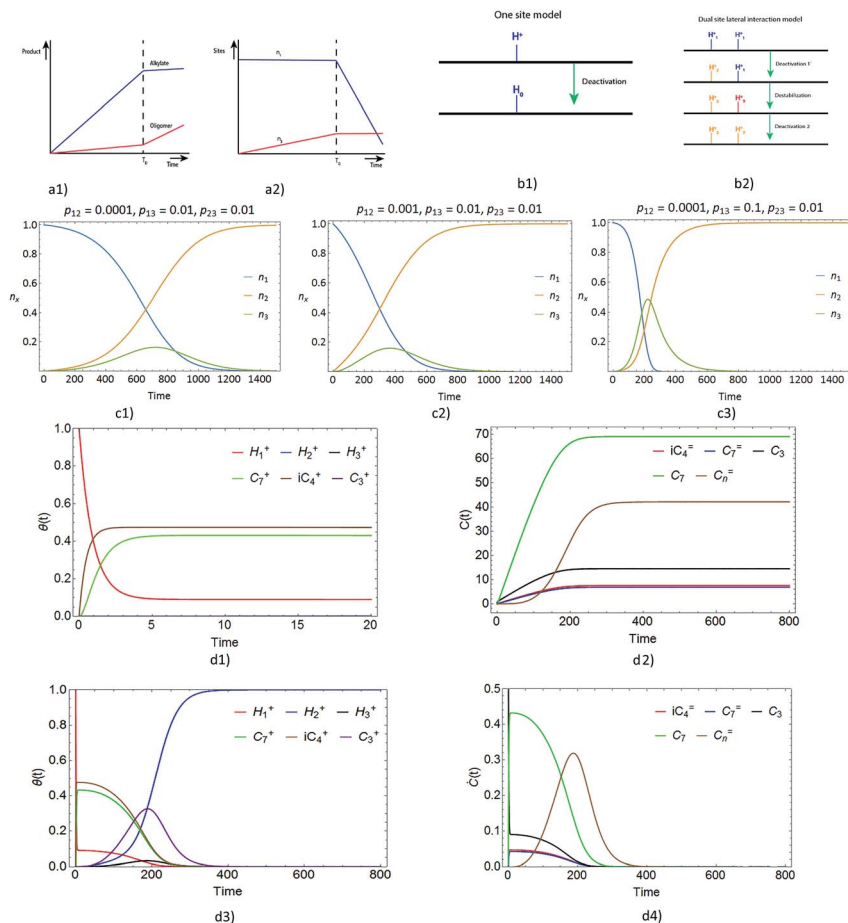


Fig. 2 Kinetic simulation according to the catalytic reaction cycle of the alkylation reaction of Fig. 1. There is one type of proton. Figures (a), (b) and (c) show the change in relative surface concentrations of  $iC_4^+$ ,  $C_7^+$ , free proton sites  $H^+$  and deactivated proton  $H_0^+$  at different timescales: (a) timescale 10; (b) timescale 100; (c) timescale 1000. Default reaction rate parameter values are  $k_1 = 1 = k_2 = k_3 = 1$ ,  $k_4, k_5 = 0.1$ ,  $k_6, k_7 = 0.01$ ; concentration parameters are  $[C_3^-] = [iC_4^-] = 1$ .



**Fig. 3** (a) Schematic product formation and site development according to experiment by Feller *et al.*;<sup>23</sup> (b) schematic illustration of the deactivation according to the one proton site (b1) and dual site interacting proton site (b2) models; (c) simulations of the time development of proton state probabilities  $n_1$ ,  $n_2$  and  $n_3$ .  $p_{12}$ ,  $p_{13}$  and  $p_{23}$  are rate constants as indicated in eqn (2). Figures (c1) and (c2) compare the effect of changes in the ratio  $p_{12}/p_{13}$ . Figure (c3) compares a change in the ratio  $p_{13}/p_{23}$ ; (d) surface intermediate concentrations and product distributions as a function of time for the alkylation reaction cycle according to the two proton lateral interaction model of figure (b2). Figures (d1) and (d3) show surface reaction intermediate concentration at short and long timescales, respectively.  $C_3^+$  is the propyl cation concentration adsorbed to the proton in state  $H_3^+$ . Figures (d2) and (d4) show as a function of time the product distributions and rates of change in product distributions also at short and long timescales, respectively. Compared to the products in Fig. 2  $C_n^-$  appears as an additional product. Rate parameters labelled according to Fig. 1:  $k_1 = k_2 = k_4 = 1$ ,  $k_3 = k_5 = 0.1$ ,  $k_6 = k_7 = 0.001$ . Reaction rate parameter of  $H_1^+$  to  $H_3^+$  conversion is 1, the reaction rates of olefin protonation and oligomerization catalyzed by  $H_3^+$  have been set equal to 0.1 and that of deactivation by oligomerization to 0.01.

Elegant experimental studies by Feller *et al.*<sup>23</sup> have demonstrated that after a finite reaction time the rate of alkylate formation suddenly stops. Usually such rapid deactivation is explained by pore blocking of the zeolite micropores due to

internal or external coke deposition. Feller *et al.* reject this possibility because the oligomerization continues. They suggest that two protons of different reactivity are involved.

The site interaction model that we present is based on that suggestion and indeed shows autocatalytic deactivation when the reactivity of the protons decreases upon deactivation. This deactivation mechanism is related also to the proposal by ref. 25 that after an initial slow deactivation, a more rapid deactivation occurs due to the onset of rapid oligomerization.

In Fig. 3a1, we have schematically sketched the alkylate and alkene production rates as experimentally observed. In the Continuous Stirred Tank Reactor (CSTR) experiment, we see an initial linear increase in alkylate production that stops after approximately 10 hours, but alkene production continues. In Fig. 3a2 we have sketched what this means for the availability of reactive proton sites.

To explain the sudden drop, we have to introduce two coupled deactivating reactions. We model this here by protons that get a different reactivity when their neighbors are isolated. In this lateral interaction model there are two kinds of proton sites: a reactive proton that catalyzes production of alkylates and is slowly consumed by deactivating reactions, and a less reactive one that cannot catalyze alkylation, but only catalyzes olefin oligomerization. Oligomerization of alkenes deactivates these sites. The deactivation rate of acidic protons by oligomerization tends to be faster than the deactivation rate by the alkylation related deactivation reactions that are activated by carbenium ion deprotonation.<sup>21</sup>

Once one proton is consumed, a negative charge builds on the zeolite framework that deactivates a neighboring proton. Such a difference in reactivity of protons is well known and is also observed when protonic zeolites become partially exchanged with alkali cations.<sup>26</sup> This is sketched in Fig. 3b.

The mean field equations of a model that simulates the interaction between the two protons as a function of their decay rate are given by eqn (2):

$$\frac{dn_1}{dt} = -p_{13}n_1 - p_{12}n_1n_2 \quad (2a)$$

$$\frac{dn_2}{dt} = p_{13}n_1 + p_{23}n_3 \quad (2b)$$

$$\frac{dn_3}{dt} = -p_{23}n_3 + p_{12}n_1n_2 \quad (2c)$$

In these equations,  $n_1$ ,  $n_2$  and  $n_3$  represent the respective proton state probabilities of protons  $H_1^+$ ,  $H_2^+$  and  $H_3^+$ :  $H_1^+$  is the proton state that catalyzes alkylation,  $H_2^+$  the deactivated non-reactive state and  $H_3^+$  the proton state that cannot catalyze alkylation, but will only oligomerize deactivating alkenes.

In Fig. 3c two representative results of the time dependence of the three proton state probabilities are shown.

The ratio  $p_{12}/p_{23}$  determines the relative amount and rate at which site  $H_3^+$  is generated. It is the ratio of the rate of  $H_3^+$  generation *versus* its lifetime. The deactivation rate of the state  $H_3^+$  has to be slow enough to obtain a high and delayed concentration of the  $H_3^+$  protons. The rate of change of proton sites  $H_1^+$  relates to the ratio of  $p_{13}/p_{23}$ . When this ratio is small, the generation rate of sites

$H_3^+$  is fast compared to the decay rate of protons  $H_1^+$ . In Fig. 3c the effect of variation of the ratio  $p_{12}/p_{23}$  on the rate of change of proton state probabilities  $n_1$ ,  $n_2$  and  $n_3$  is compared.

Fig. 3d shows simulated kinetics when the rates of change of different proton states of eqn (2) are incorporated into the kinetics equations that correspond to the reaction mechanism of Fig. 1. Proton sites  $H_1^+$  are deactivated by processes initiated by alkylate formation, sites  $H_3^+$  only catalyze oligomerization of olefins and are deactivated by subsequent processes. Time development at short and long timescales of reaction intermediates and products are shown.

When the lifetime of the  $H_3^+$  is long enough, alkene formation by oligomerization of propylene is promoted. It will continue beyond the time that  $C_7$  production has declined. This situation is illustrated in Fig. 3d4. As illustrated by Fig. 3c, when uncoupled the decay rate of alkylate can be slow compared to that due to oligomerization, whereas, when coupled, this reverses when the transformation of state  $H_1^+$  to  $H_3^+$  is fast. Catalyst lifetime is extended when the rate of  $H_3^+$  state generation decreases as happens when  $H_3$  sites become more isolated. A more extensive analysis of this model will appear in a forthcoming paper.<sup>27</sup>

The lateral interaction model of decaying sites can be considered the analogue of a Kirchhoff electrical circuit with the decay rates replaced by resistances. The rate of deactivation of the  $H_1^+$  sites increases due to the large decrease in resistance due to the opening of the deactivation channel *via* the  $H_3^+$  proton state. Catalyst deactivation in the absence of pore diffusion has rarely been investigated experimentally. An important exception is the paper by Mores *et al.*<sup>28</sup> that reports detailed experimental deactivation studies of the Methanol to Olefin (MTO) reaction in large ZSM-5 crystallites. In this reaction, the rate of deactivation is found to be substantially slower at a low proton concentration where protons become isolated.

### 3 Surface reconstruction, the Fischer–Tropsch reaction

When catalysis occurs by a transition metal particle, its surface may convert into a carbided, nitrided, sulfidic or oxidized state dependent on the reactants.

Prediction on catalyst reactivity–structure relations requires knowledge of the reaction mechanism of a reaction, as well as the state of the surface during catalytic reactions. This is particularly the case for the Fischer–Tropsch reaction. Wilson *et al.*<sup>29</sup> demonstrated that a single crystal Ru surface undergoes surface reconstruction during the Fischer–Tropsch reaction. Here we will discuss simulations of surface reconstruction of Fischer–Tropsch catalysts and discuss their relevance in relation to understanding of the reaction mechanism of Fischer–Tropsch catalysis.

In the Fischer–Tropsch reaction, synthesis gas, which consists mainly of CO and  $H_2$ , is converted into long chain hydrocarbons that are useful to gasoline production.

There is an ongoing debate on the mechanism of this reaction, that we will shortly highlight here to illustrate the relevance to establishing the reaction mechanism so as to predict the catalyst performance–structure relationship.

One of the key reaction rate relations that controls the selective production of long hydrocarbon chains is the rate of the CO bond cleavage reaction *versus*

hydrogenation of hydrocarbon intermediates adsorbed to the transition metal surface. The rate of CO bond cleavage has to be fast compared to the hydrogenation reaction, according to one school of thought.<sup>30</sup> Step-edge sites, that provide low activation sites for CO bond cleavage, are therefore essential for high chain growth selectivity. The opposing opinion is that Fischer–Tropsch catalysis occurs on the dense terraces of the catalyst.<sup>31,32</sup> In the former case the reaction may be expected to be particle size dependent. In the latter case no such dependence is expected.

In favor of the latter, it has been suggested that the high surface coverage of CO poisons the step-edge sites and that low activation energy C–O bond cleavage at the dense surface is possible since surface vacancies are readily formed by desorption of more weakly bonded CO. An alternative to this view is the calculation by Copéret *et al.*,<sup>34</sup> that shows a reaction at step-edge sites, even at high CO coverage, since H atoms remain adsorbed near the step-edges that activate CO by attachment to its O atom.

The experimental observation that water promotes catalyst reactivity has been explained by promotion of CO dissociation by H<sub>2</sub>O. This will lower the activation energy of CO dissociation on a terrace surface. It is consistent with the suggestion that terrace sites promote Fischer–Tropsch catalysis.<sup>55</sup>

However water also promotes the reactivity for a different reason. The presence of water in the reaction mixture also assists hydrogenation of adsorbed O adatoms from the surface, because hydration of adsorbed O converts it into readily removable OH adsorption intermediates.

That oxygen atom adsorption plays an important and limiting role in the Fischer–Tropsch reaction can be deduced from simulation results<sup>33</sup> as presented in Fig. 4, that show computational investigations of the optimum chain growth selectivity of the Fischer–Tropsch reaction as a function of adatom M–C and M–O bond energies. It allows for an investigation of the adsorbate surface layer composition that develops by reaction.

Three different surface reactivity regions can be distinguished; mainly O covered, mainly C covered and mainly CO covered. Optimum catalyst performance is found where the three regions meet. At the optimum reactivity, the reaction rate constants of chain growth and CH<sub>x</sub> formation by dissociation of CO compete and adsorbate vacancy surface concentration is low enough that rate of CO dissociation is fast.<sup>35</sup> The experimental system operates at the border of the O covered and CO covered surface regions.

It has also been observed experimentally for Co as well Ru, that optimum reactivity is found for catalyst particles larger than approximately 6 nm.<sup>36,37</sup>

Surface reconstruction of Co or Ru due to C atoms deposited during catalysis on or below the catalyst surface essentially influences catalyst-performance prediction. The corresponding structural changes and the inorganic chemistry that leads to such changes is little understood, but some progress has been recently made.

Quantum-chemical simulations for dense surfaces of Co<sup>38–40</sup> show that when C atoms adsorb, surface atoms rearrange in a configuration known for the more open transition metal surfaces. Within the dense surface layer, this creates a high surface transition metal atom density. The resulting strain can only be released when transition metal atoms are lifted out of the surface. This creates on the

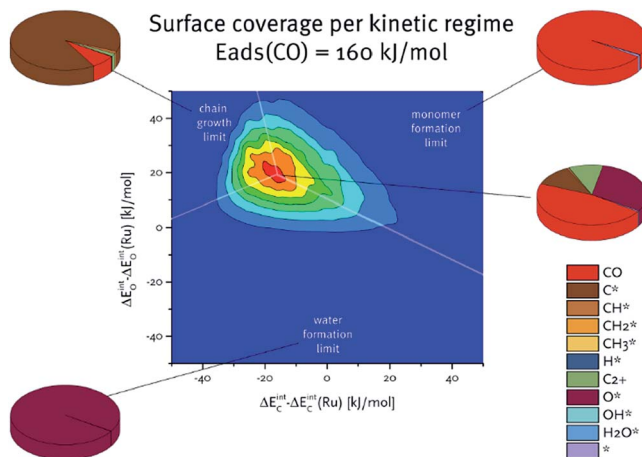


Fig. 4 Volcano plot of the rate of CO consumption as a function of M–C and M–O bond energies. The surface compositions of the three surface coverage regions are indicated. In the monomer limit region, chain growth probability increases with M–C and M–O bond energies. In the chain growth limit region it decreases because equilibrium shifts to the shorter chain lengths (Filot *et al.*<sup>33</sup>).

originally dense surface terrace step-edge sites of the kind that have low activation energy for CO bond cleavage.

Molecular dynamics simulations with ReaxFF (reactive force fields), derived by fitting with quantum-chemically calculated structures, are necessary to show these large structural changes since they can overcome the energy barriers of such reconstruction processes. Results of such simulations are shown in Fig. 5.

Particles have to be large enough so that strain due to incorporation of the C atoms into the surface is not released otherwise. Therefore on small particles C adatom adsorption generates no step-edge sites.<sup>41</sup>

This surface reorganization supports the view that step-edge sites are responsible for Fischer–Tropsch catalysis on the large particles as experimentally observed.

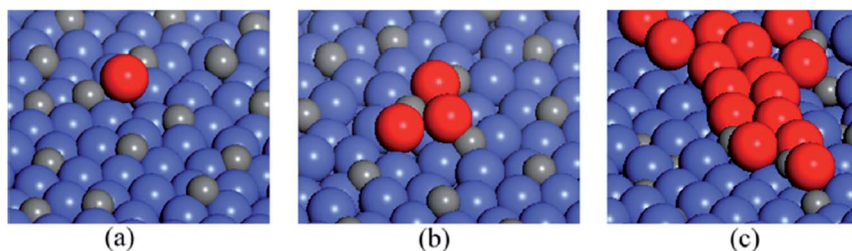


Fig. 5 Molecular dynamics simulations of carbon-induced surface transformations of Co(0001) at a temperature of 1700 K: (a) short time simulation (0.01 ns); (b) longer time simulations (0.03 ns); (c) geometry after 0.5 ns of simulation. The initial C coverage is 12.5% of the 3-fold sites. The carbon atoms are shown in gray, cobalt atoms in blue, and pop-up cobalt atoms in red.<sup>61</sup>

The main reason this mechanistic debate has not been settled by first principles theory is that microkinetic simulations including chain growth are rare. It is also essential to include lateral interactions between adsorbates since the overlayer concentration is usually high. This cannot be readily done by microkinetics simulations, since they are based on the mean field approximation. It can be more readily done with Kinetic Monte Carlo studies,<sup>42</sup> that are however not yet well suited for simulation of complex kinetics.

Promotion of the catalysts by reducible oxides as for the Co catalyst by Mn-oxide<sup>43</sup> or S and alkali for Fe catalysts<sup>44</sup> has a large effect on catalyst selectivity. There is a need to develop improved computational methods to predict the inorganic chemical changes of the complex surface chemistry that is involved.

## 4 Discussion and conclusion: controversies on reaction mechanism and structure/composition dependence

### 4.1 Reactivity descriptors

Often used reactivity descriptors in transition metal catalysis are the adsorption energies of the adatoms that are intermediates in a catalytic reaction.<sup>45</sup>

Adsorption energies of adatoms relate to the electronic structure of materials. Their d-valence electron band electron occupation and average position of the d-valence electron energy can also be used as a reactivity descriptor. This justifies having plots of reactivity against the position of a transition metal atom in a row of the periodic system. This is useful for prediction of catalyst reactivity–composition relations.

Often a volcano dependence of catalyst performance *versus* surface reactivity descriptor value is found. Microkinetics simulations that produce such volcano curves are essentially extrapolations. In these simulations, it is assumed that the surface structure does not change. Calculated elementary reaction rate data obtained for one system are correlated with elementary reaction rates of the other system through bond order conservation-type scaling rule relations between adsorbates and Brønsted–Evans–Polanyi linear activation energy–reaction energy relations.<sup>7,8</sup>

There can be two different reasons for the maximum in the volcano curve. The maximum is found where competing surface reactions balance. This is, for instance, the case of the Fischer–Tropsch example in Fig. 5 or the ammonia rate of production volcano curve plot in ref. 2.

The alternative situation is that the corresponding adatom adsorption energy has a maximum or minimum at that position. An example is the two peaked curve of electrocatalytic oxygen evolution reactivity of the perovskite oxide catalysts when plotted against the number of d-valence electrons in the periodic systems. It correlates with the electron occupation of the  $e_g$  (down)level of a transition metal cation<sup>46,47</sup> as in high spin systems. A single maximum, for which the M–O bond energy is maximum, is found when plotted against the bond energy of the M–O adsorbate bond.<sup>45</sup> This is very different for the OER curve found for the electrocatalytic reactivity of the transition metals.<sup>48</sup> Then the maximum in reactivity relates to an optimum value of the M–O bond. When the bond is too weak, M–O

bond formation becomes slow; when the M–O bond is too strong, the reaction becomes inhibited by the oxygen overlayer on the transition metal.

A similar situation arises in hydrodesulfurization catalysis.<sup>49</sup> The volcano plot maximum is found for the catalyst with the weakest M–S bond. Indeed the reaction orders do not alter left or right from the volcano curve maximum.<sup>50</sup>

Also rules have been developed that predict reactivity–surface topology relations. For instance, a chemical C–H bond that is  $\sigma$  symmetric requires only a single transition metal atom to be activated. In contrast, dissociation of the  $\pi$  symmetric C–O bond of the CO molecule requires a surface ensemble of five or six atoms preferentially located on a surface terrace of the step-edge site, to accommodate the C adatom as well as the O adatom generated by dissociation. This has led to a prediction of the dependence of the reaction rate of reaction as a function of transition metal particle size that relates to the character of the chemical bond that is activated.<sup>51</sup>

This relation of particle size dependence, site structure and orbital symmetry of chemical bond is relevant as long as other causes of chemical reactivity dependence are not present. For instance, the particle size dependence model breaks down when, because of ready carbide or oxide formation, the small particles lose their metallic nature and deactivate.<sup>49</sup>

#### 4.2 Catalytic reactivity, surface reconstruction and catalyst deactivation

To predict the rate of the catalytic reaction, microkinetics simulations are indispensable. Microkinetics simulations require knowledge of adsorption energies of reaction intermediates, which may be a strong function of surface coverage. Since the adsorbate overlayer composition at reaction conditions is usually not known *a priori*, the adsorption energies are usually calculated for an assumed reactive overlayer composition and surface structure.

The assumption that surface atom structure does not change during the reaction is not always valid. We discussed in Section 3 for the Fischer–Tropsch reaction that such structural changes not only affect predictions of reactivity–structure relations, but even predictions of the mechanism of the reaction. The structural change and reaction mechanism interconnect. The difficulty to establish this relation is an important reason why for several important catalytic reactions there is no agreement on their reactivity–structure/composition relation.

An additional example is provided by the ethylene epoxidation reaction catalyzed by silver. There is no consensus whether the catalyst surface is to be considered metallic or oxidic. On the metallic transition metal surface, the epoxide is formed through an oxo-metallo cycle intermediate.<sup>52</sup> Epoxide formation has a slightly higher activation energy compared with the non-selective acetaldehyde coproduct. Interestingly the reverse situation is found for epoxidation catalyzed by the Cu surface. Therefore in contrast to the catalytic experiment, instead of Ag, Cu is predicted to be the more selective one.

The prediction of catalyst selectivity is different when reaction on the silver oxide surface is compared with that on the copper oxide. Then no oxo-metallo cycle is formed, but epoxidation occurs by direct reaction of ethylene with a surface oxygen atom. In this case, selectivity to form the epoxide is the highest on the silver oxide instead of copper oxide.<sup>53</sup> The state of the catalyst

surface not only affects the reaction mechanism, but also the reactivity–composition relationship. Since the oxide layer is not stable under reaction conditions, promoters such as Cl and alkali are added to the catalyst, but their action is little understood as yet, which relates to the difficult problem to predict the structure of a complex inorganic surface.

Also in zeolite catalysis the structure of the catalytically reactive sites may change during the reaction. This has been found for oxycationic clusters located in the zeolite cavity, for example, the  $\text{GaOGa}(\text{OH})^{2+}$  complex catalyzes alkane dehydrogenation, but this reaction competes with water formation by reaction of H atoms with the O atom, which deactivates the catalyst.<sup>54</sup> Also, as in the Panov reaction, framework cations will move out of the framework into the zeolite microchannel as oxycationic clusters during the reaction. The reaction cycles of product formation and deactivation are closely related. In the case of the Panov reaction, the stability of the catalyst depends strongly on the catalytically active cationic species.<sup>55</sup>

### 4.3 Quantitative prediction?

Accurate reaction rate prediction requires an accuracy of reaction intermediate prediction of  $\text{kJ mol}^{-1}$ , that is beyond the reach of currently available periodic quantum-chemical DFT approaches that are the working horse of computational catalysis.

Remarkably microkinetics simulations of overall reaction rates of catalytic reactions agree much better with experiment than might be expected. The reason for this is that adsorption energies of reaction intermediates and corresponding elementary reaction rate activation energies are correlated, through linear activation energy–reaction energy Brønsted–Evans–Polanyi relations. It causes a partial cancellation of systematic errors.

However this error cancellation does not apply for the adsorption and desorption rates of reactants or products between the reaction medium and catalyst surface on which the overlayer concentration sensitively depends. Since this may strongly affect the temperature of the simulated reaction, kinetic simulations sometimes require adjustment of the computed adsorption energies.

Eyring transition state theory is usually used to calculate elementary reaction rate constants. It applies when reaction barriers can be considered isolated and energy exchange between adsorbed reactants and catalyst surface is fast compared to that of the corresponding elementary reactions. Zero Kelvin transition states computed in stationary DFT quantum-chemical methods have been found not to apply when in the activated state the system contains several close local stationary minima. Then advanced molecular dynamics methods, such as metadynamics methods, have to be applied (see ref. 56).

For zeolites, mobility of protonated intermediates is so high that carbenium ions change from transition states to stable mobile intermediates.

Another interesting example where use of metadynamics approaches have led to a new view on the transition state intermediates is proton activation of alkanes through formation of intermediate carbonium ion formation (see Fig. 6).

It compares transition states according to the early Haag–Gates<sup>57</sup> proposal of carbonium ion formation based on alkane fragmentation kinetics by protons as discovered in cyclotrons (Fig. 6a), with zero Kelvin calculated carbonium ion

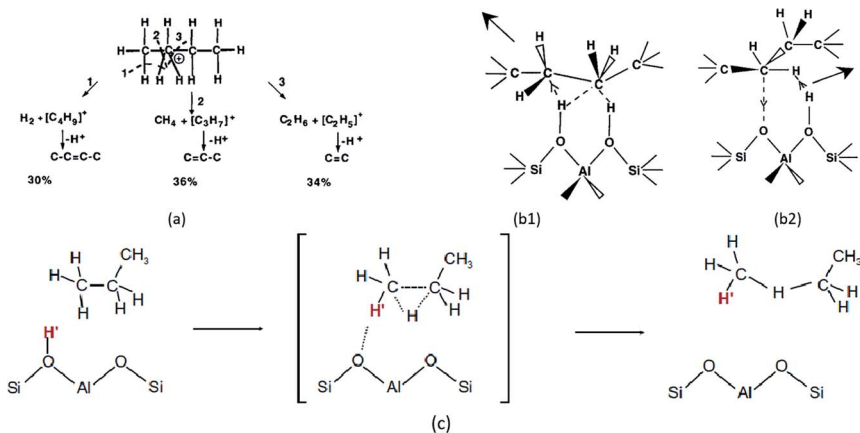


Fig. 6 Comparison of three transition state models of proton activated alkane cracking. (a) Schematic representation of the Haag–Gates<sup>57</sup> intermediate carbonium ion decomposition model. (b) Schematic representation of the carbonium ion transition model by Lercher *et al.*<sup>58</sup> (b1) activation of C–C bond; (b2) activation of C–H bond. The proton activates directly the hydrocarbon bond that decomposes. (c) Schematic representation of the indirect carbonium ion transition model by Bucko *et al.*<sup>59</sup>

transition states for this reaction (Fig. 6b).<sup>58</sup> Since there is strong electrostatic interaction between the protonated molecule and the negative charge left on the zeolite lattice, the transition state “knows” of the vacant site and is unique for each bond to be activated. Interestingly, using advanced molecular dynamics techniques it has recently been discovered that the actual reaction paths may be inbetween the two extremes of Fig. 6a and b. The initial attachment may occur to a C–H bond but the proton may then move to the next C–C bond.<sup>59,60</sup>

Further use of such methods promises a great number of new elementary reaction paths and will substantially affect mechanistic proposals of heterogeneous catalytic reactions.

#### 4.4 In conclusion

Computational tools have become available that make possible simulation of first principle kinetics of catalytic reactions based on catalyst structure and composition close to that of experimental systems.

Key for proper prediction of reaction performance–catalyst structure/composition relations is prediction of the right reaction mechanism in the different stages of the catalytic reaction process, *i.e.* initiation, propagation and deactivation. A fundamental problem to be resolved for each catalytic system is the state of the catalysts under reaction conditions and how this relates to its reaction mechanism. There is as yet no standard approach for this and simulations depend on comparative choices on reaction mechanism and often assumptions on catalyst structure and composition.<sup>7</sup> It is the reason for the many open controversies that still exist on the mechanisms of important heterogeneous catalytic reactions.

The ultimate challenge to the prediction of catalytic reactivity is to overcome the difficulty that the state of catalysts and catalytic reaction mechanism are interdependent and self-refer to each other.

# Conflicts of interest

There are no conflicts to declare.

## Acknowledgements

A. Sengar acknowledges support from the NWO-MCEC program. E. Steur acknowledges support from the ICMS Institute of the Technical University Eindhoven.

## Notes and references

- 1 O. Novaro, E. Blaisten-Barojas, E. Clementi, G. Giunchi and M. E. Ruiz-Vizcaya, Theoretical study on a reaction pathway of Ziegler–Natta-type catalysis, *J. Chem. Phys.*, 1978, **68**, 2337–2351, DOI: 10.1063/1.436004.
- 2 S. Dahl, A. Logadottir, C. J. H. Jacobsen and J. K. Nørskov, Electronic factors in catalysis: the volcano curve and the effect of promotion in catalytic ammonia synthesis, *Appl. Catal., A*, 2001, **222**, 19–29, DOI: 10.1016/S0926-860X(01)00826-2.
- 3 D. W. Lewis, D. J. Willock, C. R. A. Catlow, J. M. Thomas and G. J. Hutchings, De novo design of structure-directing agents for the synthesis of microporous solids, *Nature*, 1996, **382**, 604–606, DOI: 10.1038/382604a0.
- 4 W. A. Goddard, A. van Duin, K. Chenoweth, M.-J. Cheng, S. Pudar, J. Oxgaard, B. Merinov, Y. H. Jang and P. Persson, Development of the ReaxFF reactive force field for mechanistic studies of catalytic selective oxidation processes on BiMoO<sub>x</sub>, *Top. Catal.*, 2006, **38**, 93–103, DOI: 10.1007/s11244-006-0074-x.
- 5 K. Chenoweth, A. C. T. van Duin, P. Persson, M.-J. Cheng, J. Oxgaard and W. A. Goddard, Development and Application of a ReaxFF Reactive Force Field for Oxidative Dehydrogenation on Vanadium Oxide Catalysts, *J. Phys. Chem. C*, 2008, **112**, 14645–14654, DOI: 10.1021/jp802134x.
- 6 P. Stoltze, Microkinetic simulation of catalytic reactions, *Prog. Surf. Sci.*, 2000, **65**, 65–150.
- 7 R. A. van Santen, *Modern Heterogeneous Catalysis: An Introduction*, Wiley VCH, 2017.
- 8 J. K. Nørskov, F. Studt, F. Abild-Pedersen, and T. Bligaard, *Fundamental Concepts in Heterogeneous Catalysis*, Wiley, 2014.
- 9 V. Van Speybroeck, K. Hemelsoet, L. Joos, M. Waroquier, R. G. Bell and C. R. A. Catlow, Advances in theory and their application within the field of zeolite chemistry, *Chem. Soc. Rev.*, 2015, **44**, 7044–7111.
- 10 G. Piccini, M. Alessio and J. Sauer, *Ab Initio* Calculation of Rate Constants for Molecule-Surface Reactions with Chemical Accuracy, *Angew. Chem., Int. Ed.*, 2016, **55**, 5235–5237, DOI: 10.1002/anie.201601534.
- 11 C. Tuma and J. Sauer, Treating dispersion effects in extended systems by hybrid MP2:DFT calculations—protonation of isobutene in zeolite ferrierite, *Phys. Chem. Chem. Phys.*, 2006, **8**, 3955–3965.
- 12 A. T. Bell and M. Head-Gordon, Quantum Mechanical Modeling of Catalytic Processes, *Annu. Rev. Chem. Biomol. Eng.*, 2011, **2**, 453–477, DOI: 10.1146/annurev-chembioeng-061010-114108.

- 13 C. R. A. Catlow, V. Van Speybroeck, and R. A. van Santen, *Modelling and Simulation in the Science of Micro- and Meso-Porous Materials*, Elsevier, 2017.
- 14 C. Stampfl, H. J. Kreuzer, S. H. Payne, H. Pfnür and M. Scheffler, First-Principles Theory of Surface Thermodynamics and Kinetics, *Phys. Rev. Lett.*, 1999, **83**, 2993–2996, DOI: 10.1103/PhysRevLett.83.2993.
- 15 B. Smit and T. L. M. Maesen, Molecular Simulations of Zeolites: Adsorption, Diffusion, and Shape Selectivity, *Chem. Rev.*, 2008, **108**, 4125–4184, DOI: 10.1021/cr8002642.
- 16 J. F. Haw, W. Song, D. M. Marcus and J. B. Nicholas, The Mechanism of Methanol to Hydrocarbon Catalysis, *Acc. Chem. Res.*, 2003, **36**, 317–326, DOI: 10.1021/ar020006o.
- 17 H. Kranilla, Monomolecular and bimolecular mechanisms of paraffin cracking: *n*-butane cracking catalyzed by HZSM-5, *J. Catal.*, 1992, **135**, 115–124, DOI: 10.1016/0021-9517(92)90273-K.
- 18 A. Corma and A. Martinez, Chemistry, Catalysts, and Processes for Isoparaffin–Olefin Alkylation: Actual Situation and Future Trends, *Catal. Rev. Sci. Eng.*, 1993, **35**, 483–570.
- 19 L. Schmerling, The Mechanism of the Alkylation of Paraffins. II. Alkylation of Isobutane with Propene, 1-Butene and 2-Butene, *J. Am. Chem. Soc.*, 1946, **68**, 275–281, DOI: 10.1021/ja01206a038.
- 20 C. R. A. Catlow, V. Van Speybroeck, and R. A. Van Santen, in *Modelling and Simulation in the Science of Micro- and Meso-Porous Materials*, Elsevier, 2017, ch. 5.
- 21 C. Liu, R. A. van Santen, A. Poursaeidesfahani, T. J. H. Vlugt, E. A. Pidko and E. J. M. Hensen, Hydride Transfer versus Deprotonation Kinetics in the Isobutane–Propene Alkylation Reaction: A Computational Study, *ACS Catal.*, 2017, **7**, 8613–8627, DOI: 10.1021/acscatal.7b02877.
- 22 L. Schmerling, The Mechanism of the Alkylation of Paraffins, *J. Am. Chem. Soc.*, 1945, **67**, 1778–1783, DOI: 10.1021/ja01226a048.
- 23 A. Feller, A. Guzman, I. Zuazo and J. A. Lercher, On the mechanism of catalyzed isobutane/butene alkylation by zeolites, *J. Catal.*, 2004, **224**, 80–93.
- 24 U. Olsbye, S. Svelle, M. Bjrgen, P. Beato, T. V. W. Janssens, F. Joensen, S. Bordiga and K. P. Lillerud, Conversion of methanol to hydrocarbons: How zeolite cavity and pore size controls product selectivity, *Angew. Chem., Int. Ed.*, 2012, **51**, 5810–5831.
- 25 K. P. de Jong, C. M. A. M. Mesters, D. G. R. Peferoen, P. T. M. van Brugge and C. de Groot, Paraffin alkylation using zeolite catalysts in a slurry reactor: Chemical engineering principles to extend catalyst lifetime, *Chem. Eng. Sci.*, 1996, **51**, 2053–2060.
- 26 E. G. Derouane, J. C. Védrine, R. R. Pinto, P. M. Borges, L. Costa, M. A. N. D. A. Lemos, F. Lemos and F. R. Ribeiro, The Acidity of Zeolites: Concepts, Measurements and Relation to Catalysis: A Review on Experimental and Theoretical Methods for the Study of Zeolite Acidity, *Catal. Rev. Sci. Eng.*, 2013, **55**, 454–515, DOI: 10.1080/01614940.2013.822266.
- 27 R. A. van Santen, E. Steur and A. Sengar, 2017, in preparation.
- 28 D. Mores, J. Kornatowski, U. Olsbye and B. M. Weckhuysen, Coke Formation during the Methanol-to-Olefin Conversion: *In Situ* Microspectroscopy on Individual H-ZSM-5 Crystals with Different Brønsted Acidity, *Chem.–Eur. J.*, 2011, **17**, 2874–2884.

- 29 J. H. Wilson and C. P. M. de Groot, *J. Phys. Chem.*, 1995, **99**, 7860–7866.
- 30 R. A. van Santen, A. J. Markvoort, I. A. W. Filot, M. M. Ghouri and E. J. M. Hensen, Mechanism and microkinetics of the Fischer–Tropsch reaction, *Phys. Chem. Chem. Phys.*, 2013, **15**, 17038.
- 31 M. Ojeda, R. Nabar, A. U. Nilekar, A. Ishikawa, M. Mavrikakis and E. Iglesia, CO activation pathways and the mechanism of Fischer–Tropsch synthesis, *J. Catal.*, 2010, **272**, 287–297.
- 32 D. D. Hibbitts, B. T. Loveless, M. Neurock and E. Iglesia, Mechanistic role of water on the rate and selectivity of Fischer–Tropsch synthesis on ruthenium catalysts, *Angew. Chem., Int. Ed.*, 2013, **52**, 12273–12278.
- 33 I. A. W. Filot, R. A. van Santen and E. J. M. Hensen, The optimally performing Fischer–Tropsch catalyst, *Angew. Chem., Int. Ed.*, 2014, **53**, 12746–12750, DOI: 10.1002/anie.201406521.
- 34 L. Foppa, C. Copéret and A. Comas-Vives, Increased Back-Bonding Explains Step-Edge Reactivity and Particle Size Effect for CO Activation on Ru Nanoparticles, *J. Am. Chem. Soc.*, 2016, **138**, 16655–16668, DOI: 10.1021/jacs.6b08697.
- 35 R. A. van Santen, A. J. Markvoort, M. M. Ghouri, P. A. J. Hilbers and E. J. M. Hensen, Monomer Formation Model *versus* Chain Growth Model of the Fischer–Tropsch Reaction, *J. Phys. Chem. C*, 2013, **117**, 4488–4504.
- 36 J. P. den Breejen, G. L. Bezemer, J. H. Bitter, V. Frøseth, A. Holmen, K. P. Jong and P. B. Radstake, *J. Am. Chem. Soc.*, 2009, **131**, 7197–7203.
- 37 G. L. Bezemer, H. P. C. E. Kuipers, H. Oosterbeek, J. E. Holewijn, X. Xu, F. Kapteijn, A. K. van Dillen, K. P. de Jong and J. H. Bitter, Cobalt particle size effects in the Fischer–Tropsch reaction studied with carbon nanofiber supported catalysts, *J. Am. Chem. Soc.*, 2006, **128**, 3956.
- 38 I. M. Ciobică, R. A. van Santen, P. J. van Berge and J. van de Loosdrecht, Adsorbate induced reconstruction of cobalt surfaces, *Surf. Sci.*, 2008, **602**, 17–27.
- 39 I. M. Ciobică, P. Van Helden and R. A. Van Santen, Stability and effects of carbon-induced surface reconstructions in cobalt Fischer–Tropsch synthesis, *Surf. Sci.*, 2016, **653**, 82–87.
- 40 M. Corral Valero and P. Raybaud, Stability of carbon on cobalt surfaces in Fischer–Tropsch reaction conditions: A DFT study, *J. Phys. Chem. C*, 2014, **118**, 22479–22490.
- 41 X.-Q. Zhang, E. Iype, S. V. Nedeia, A. P. J. Jansen, B. M. Szyja, E. J. M. Hensen and R. A. van Santen, Site Stability on Cobalt Nanoparticles: A Molecular Dynamics ReaxFF Reactive Force Field Study, *J. Phys. Chem. C*, 2014, **118**, 6882–6886, DOI: 10.1021/jp500053u.
- 42 R. A. van Santen, S. Shetty, E. J. M. Hensen and M. M. Ghouri, Structure sensitivity of the Fischer–Tropsch reaction; molecular kinetics simulations, *Catal. Sci. Technol.*, 2011, **1**, 891–911.
- 43 Y. Xiang and N. Kruse, Tuning the catalytic CO hydrogenation to straight- and long-chain aldehydes/alcohols and olefins/paraffins, *Nat. Commun.*, 2016, **7**, 13058.
- 44 H. M. Torres Galvis, J. H. Bitter, C. B. Khare, M. Ruitenbeek, A. I. Dugulan and K. P. de Jong, Supported Iron Nanoparticles as Catalysts for Sustainable Production of Lower Olefins, *Science*, 2012, **335**, 835–838, DOI: 10.1126/science.1215614.

- 45 A. Vojvodic and J. K. Nørskov, Optimizing Perovskites for the Water-Splitting Reaction, *Science*, 2011, **334**, 1355, DOI: 10.1126/science.1215081.
- 46 J. Suntivich, H. A. Gasteiger, N. Yabuuchi, H. Nakanishi, J. B. Goodenough and Y. Shao-Horn, Design principles for oxygen-reduction activity on perovskite oxide catalysts for fuel cells and metal-air batteries, *Nat. Chem.*, 2011, **3**, 647, DOI: 10.1038/nchem.1093.
- 47 J. Suntivich, K. J. May, H. A. Gasteiger, J. B. Goodenough and Y. Shao-Horn, A Perovskite Oxide Optimized for Oxygen Evolution Catalysis from Molecular Orbital Principles, *Science*, 2011, **334**, 1383–1385, DOI: 10.1126/science.1212858.
- 48 I. C. Man, H.-Y. Su, F. Calle-Vallejo, H. A. Hansen, J. I. Martínez, N. G. Inoglu, J. Kitchin, T. F. Jaramillo, J. K. Nørskov and J. Rossmeisl, Universality in Oxygen Evolution Electrocatalysis on Oxide Surfaces, *ChemCatChem*, 2011, **3**, 1159–1165, DOI: 10.1002/cctc.201000397.
- 49 H. W. Kouwenhoven and W. C. van Zijll Langhout, Hydroisomerisation catalysis, *Chem. Eng. Prog.*, 1971, **67**, 65.
- 50 D. A. J. M. Ligthart, R. A. van Santen and E. J. M. Hensen, Influence of particle size on the activity and stability in steam methane reforming of supported Rh nanoparticles, *J. Catal.*, 2011, **280**, 206–220.
- 51 R. A. Van Santen, Complementary structure sensitive and insensitive catalytic relationships, *Acc. Chem. Res.*, 2009, **42**, 57–66.
- 52 S. Linic and M. A. Barteau, Construction of a reaction coordinate and a microkinetic model for ethylene epoxidation on silver from DFT calculations and surface science experiments, *J. Catal.*, 2003, **214**, 200–212.
- 53 M. O. Özbek and R. A. van Santen, The Mechanism of Ethylene Epoxidation Catalysis, *Catal. Lett.*, 2013, **143**, 131–141.
- 54 E. J. M. Hensen, E. A. Pidko, N. Rane and R. A. Van Santen, Water-promoted hydrocarbon activation catalyzed by binuclear gallium sites in ZSM-5 zeolite, *Angew. Chem., Int. Ed.*, 2007, **46**, 7273–7276.
- 55 G. Li, E. A. Pidko, R. A. Van Santen, Z. Feng, C. Li and E. J. M. Hensen, Stability and reactivity of active sites for direct benzene oxidation to phenol in Fe/ZSM-5: A comprehensive periodic DFT study, *J. Catal.*, 2011, **284**, 194–206.
- 56 K. De Wispelaere, S. Bailleul and V. Van Speybroeck, Towards molecular control of elementary reactions in zeolite catalysis by advanced molecular simulations mimicking operating conditions, *Catal. Sci. Technol.*, 2016, **6**, 2686–2705.
- 57 H. Krannila, Monomolecular and bimolecular mechanisms of paraffin cracking: *n*-butane cracking catalyzed by HZSM-5, *J. Catal.*, 1992, **135**, 115–124.
- 58 J. A. Lercher, R. A. van Santen and H. Vinek, Carbonium ion formation in zeolite catalysis, *Catal. Lett.*, 1994, **27**, 91–96, DOI: 10.1007/BF00806981.
- 59 T. Bucko, L. Benco, J. Hafner and G. A. Janos, Monomolecular cracking of propane over acidic chabazite: An *ab initio* molecular dynamics and transition path sampling study, *J. Catal.*, 2011, **279**, 220–228.
- 60 P. M. Zimmerman, C. Tranca, J. Gomes and D. Lambrecht, *Ab Initio* Simulations Reveal that Reaction Dynamics Strongly Affect Product Selectivity for the Cracking of Alkanes over H-MFI, *J. Am. Chem. Soc.*, 2012, **134**, 19468–19476.
- 61 X.-Q. Q. Zhang, R. A. van Santen and E. J. M. Hensen, Carbon-Induced Surface Transformations of Cobalt, *ACS Catal.*, 2015, **5**, 596–601.